Journal of Southeast University (English Edition) Vol. 34, No. 4, pp. 517 - 523 Dec. 2018 ISSN 1003—7985

Spatiotemporal distribution characteristics of bridge deck runoff

Geng Yanfen Ke Xing Zheng Xin

(School of Transportation, Southeast University, Nanjing 210096, China)

Abstract: The spatiotemporal characteristics of bridge deck runoff under a natural rainfall event are explored. The Taizhou Bridge is taken as a study case, and a hydrodynamic model based on the two-dimensional shallow water equations is used to analyze the runoff characteristics. The results indicate that the runoff velocity rate and depth are positively related to rainfall intensity, yet they have different response degrees to it. The inlet's effect degree on lane water film has a positive relationship with rainfall intensity. A natural logarithm function (R^2 = 0.706) can illustrate this relationship. However, the inlet's effect degree on ponding at the curb shows a negative relationship with the rainfall intensity. A negative exponential function (R^2 = 0.824) can reveal this relationship. With the decrease in the longitudinal slope S_L, the ponding depth at the curb increases significantly at the bridge approach slab, whereas the lane water film thickness (WFT) is almost unchanged, but the lane WFT increases greatly at the location with the minimum longitudinal slope. It is concluded that the characteristics of the bridge deck runoff present apparent spatiotemporal differences, the inlet's effects on bridge deck runoff are quantitatively correlated with rainfall intensity, and the effective drainage measures are necessary for the bridge approach slab.

Key words: two-dimensional shallow water equations; bridge deck runoff; spatiotemporal characteristics; ponding depth; water film thickness

DOI: 10.3969/j.issn.1003-7985.2018.04.015

The natural rainstorm events have increased greatly in recent years, and the impacts caused by rainwater runoff has received much attention. Many runoff experiments on pavement surfaces have been carried out to study the relationship between the water film thickness (WFT) and influence factors, and the empirical equations were derived from those experiments' data[1]. The WFT can also be obtained by the BP neural network model[2]. On the basic theories of flow continuity equation and momentum equation, Chen[3] established a complex theory equation to calculate the WFT on pavement. A theoretical equation with a simple form was proposed by using the Chézy equation and Manning equation[4].

The 1D numerical model is an efficient tool to calculate the runoff depth. The variation of runoff depth was simulated under different rainfall intensities by embedding a DeSaint Venant runoff model into the SWMM model[5]. With the assumption of 1D flow conditions, the empirical PLANUS model was developed to present the water film distribution of sheet flow[6]. Kinematic wave equation acted as a governing equation in model building in the earlier study[7]. However, most of 1D models over-predicted WFT since only the bottom slope was considered, momentum and horizontal pressure gradient were ignored[8].

Runoff characteristics are also popularly presented by multi-dimensional numerical simulation. Tan et al.[9] used the SEEP 3D to analyze the effects of road geometric properties and rainfall intensity on pavement drainage characteristics. Flow 3D can simulate the flow patterns around inlets and evaluate the grated inlet performance[10]. Charbeneau et al.[11] stated that the location of the maximum ponding depth at the curb depended on the longitudinal slope at superelevation transition. Jeong et al.[12] suggested that the transverse slope, longitudinal slope, rainfall intensity and pavement width have an obvious effect on the distribution of sheet flow at superelevation transition. Ressel et al.[13] developed the pavement surface runoff model to simulate the flow of pavement surface runoff.

Most studies focused on pavement runoff distribution by using different methods, and few studies focused on the characteristics of bridge deck runoff under natural rainfall events. Due to the impermeability of bridge deck and inefficient drainage systems, bridge deck runoff is more likely to occur. However, in order to protect bridge structures, their drainage requirement must be higher than that of highways. Moreover, more instabilities and risks are aggravated by the natural rainfall intensity. Thus, it is meaningful to analyze the spatiotemporal distribution of bridge deck runoff under a natural rainfall event.

1 Methods and Materials

1.1 Numerical model

The pavement runoff is a free surface flow, and the water depth is far less than the flooded area, which matches with the applicable conditions of 2D shallow water equations. When vertical flow velocities and vertical derivatives of pavement runoff are negligible, the assump-

Received 2018-02-26, **Revised** 2018-08-13.

Biography: Geng Yanfen (1978—), female, doctor, associate professor, yfgeng@seu.edu.cn.

Foundation item: The National Natural Science Foundation of China (No. 51109039, 5147814).

Citation: Geng Yanfen, Ke Xing, Zheng Xin. Spatiotemporal distribution characteristics of bridge deck runoff[J]. Journal of Southeast University (English Edition), 2018, 34(4): 517 - 523. DOI: 10.3969/j.issn.1003-7985.2018.04.015.

tion of hydrostatic pressure can be applied to shallow water equations, which leads to the 2D depth-averaged shallow water equations:

$$\frac{\partial}{\partial t}\begin{bmatrix} h \\ uh \\ vh \end{bmatrix} + \frac{\partial}{\partial x}\begin{bmatrix} uh \\ uh^2 + \frac{1}{2}gh^2 \\ uvh \end{bmatrix} + \frac{\partial}{\partial t}\begin{bmatrix} vh \\ vuh \\ vh^2 + \frac{1}{2}gh^2 \end{bmatrix} = \begin{bmatrix} q \\ ghS_{ox} + ghS_{fx} \\ ghS_{oy} + ghS_{fy} \end{bmatrix} \quad (1)$$

where x, y are the coordinates of the pavement surface; g is the gravity constant, m/s^2; h is the water depth, m; u and v are the average velocities of x and y directions, respectively, m/s; S_{ox} and S_{oy} are the bed slope source terms; S_{fx} and S_{fy} are the friction source terms; and q is the source discharge per unit plan-surface area, m^3/s.

The unstructured finite-volume method and Roe's approximate Riemann solver are applied in this numerical model. This model is robust and can predict different types of flows including subcritical, supercritical, and transcritical flows. To validate this model, on-site measuring work was implemented in the project of the Shen-Shan expressway. The runoff depth on the expressway surface and rainfall intensity were measured. As shown in Fig. 1, the simulation result states a good consistency with the measured runoff depth on the existing pavement[14]. Thus, this model is effective.

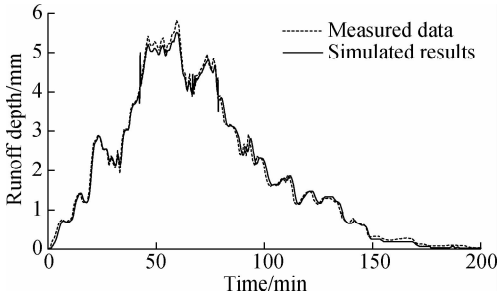

Fig. 1 Simulated results and measured data of runoff depth on the existing pavement

1.2 Study area and basic data

Connecting three big cities, the maximum traffic flow of Taizhou Bridge is about 100 thousand vehicles per day. Owing to the symmetry of the plane layout, only 1/4 bridge is simulated. Undepressed curb-opening inlets with equal spacing are set to receive bridge deck runoff. A longitudinal gutter is arranged at the longitudinal edge of the bridge to accept the flow from inlets. The specific design parameters of the numerical simulation are tabulated in Tab. 1. At the end of bridge approach slab, the highway with a length of 25 m, a longitudinal slope of 0 and a traverse slope of 2% is included in this simulation.

Tab. 1 Design parameters of numerical bridge model

Parameter	Value
Bridge length/m	1 080
Lane width/m	11.25
Undepressed inlet/(m × m × m)	0.35 × 0.1 × 1.7
Bridge width/m	19.55
Shoulder width/m	3.00
Height of curb/m	0.155
Longitudinal slope/%	2.50
Traverse slope/%	2.00

The numerical bridge model and plane layout are shown in Fig. 2. The open boundary conditions are applied to all boundaries in the simulation. The maximum cell size is 0.4 m^2; the minimum cell size is 0.01 m^2; the time step is 0.20 s; and the Manning coefficient is 0.016. Fig. 2(a) also depicts the spatial positions of sections and the measuring points which are used to analyze the bridge deck runoff, and their detail coordinates are displayed in Tab. 2 and Tab. 3.

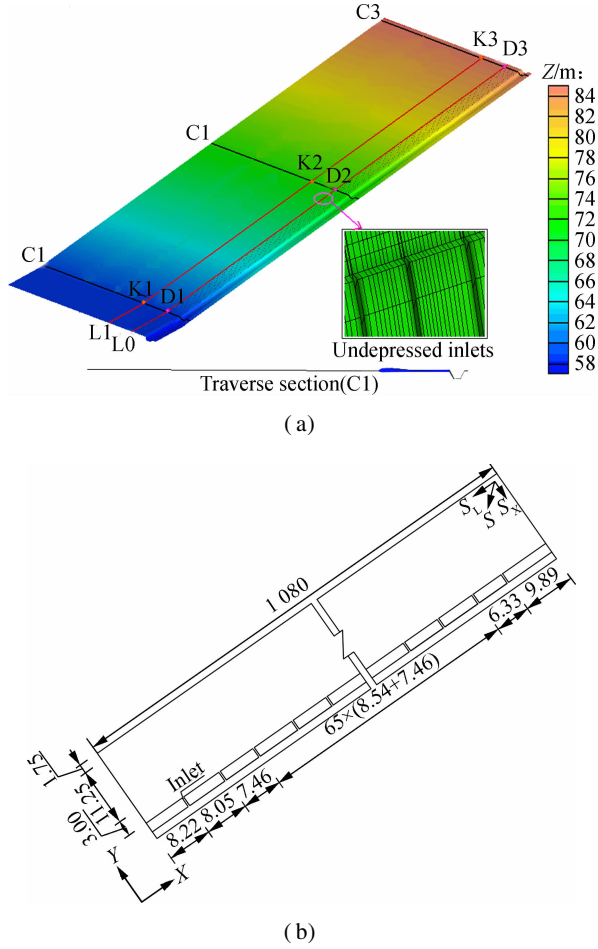

Fig. 2 Numerical model of Taizhou Bridge. (a) Numerical model and location annotation; (b) Plane layouts of bridge (unit: m)

There was a rainstorm in Taizhou on July 4, 2012. The rainfall process is shown in Fig. 3. The cumulative precipitation reached 71.50 mm, and the maximum rainfall intensity (58.20 mm/h) appeared at 03∶46. Extreme weather has become more frequent in recent years, and the

Tab. 2 Coordinates and annotations of observation sections

Section	Coordinates/m	Annotation
L0	$Y=2.075$	Curb section
L1	$Y=5.075$	The 1st lane edge
C1	$X=4$	The end of bridge
C2	$X=537$	The middle of bridge
C3	$X=1\ 069$	The top of bridge

Tab. 3 Coordinates and annotations of observation points

Point	Coordinates/(m, m)	Annotation
D1	(4, 2.075)	D1, D2 and D3 are the observation points of the ponding at curb
D2	(537, 2.075)	
D3	(1069, 2.075)	
K1	(4, 5.075)	K1, K2 and K3 are the observation points of the lane WFT
K2	(537, 5.075)	
K3	(1069, 5.075)	

natural rainfall intensity has increased significantly[15]. In order to ensure the safety margin of the system, this rainstorm event was chosen as the model dynamic boundary condition.

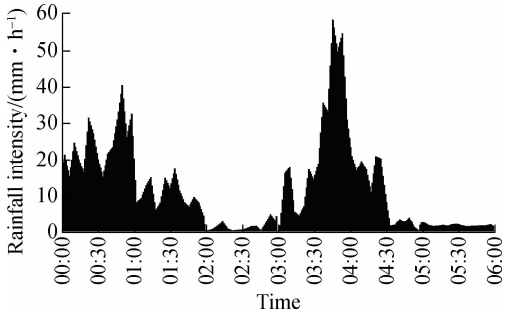

Fig. 3 Rainfall intensity on July 4, 2012

2 Results and Discussion

2.1 The temporal distribution

A significantly positive association is observed in Fig. 4 between the ponding depth at the curb and the rainfall intensity, while compared to D1 and D2, D3 is clearly lower. Meanwhile, as shown in Tab. 4, the maximum ponding depth (29.99 mm) at the curb occurs at 03:49. Fig. 5 shows gutter water surface profiles of different transverse sections at 03:49. It illustrates that the ponding width is not constant, and the maximum width is about 1.50 m (from 2.075 to 3.60 m in the X direction). The shoulder width of the bridge deck is 3.00 m, which indicates that the ponding water does not enter the lanes. Thus, the area above section L1 is the sheet flow, and the sheet flow depth is defined as WFT. The WFT of K1, K2 and K3 also displays a positive relationship with the rainfall intensity (see Fig. 6). The WFT of K1, K2 is slightly larger than that of K3, and the maximum WFT (1.64 mm) occurs at 03:47.

Tab. 4 gives the specific values of the runoff depth. There is a time interval of 1.00 min with a rainfall intensity of 58.20 mm/h between the peak of the rainfall intensity and lane WFT, which is the sheet flow travel time

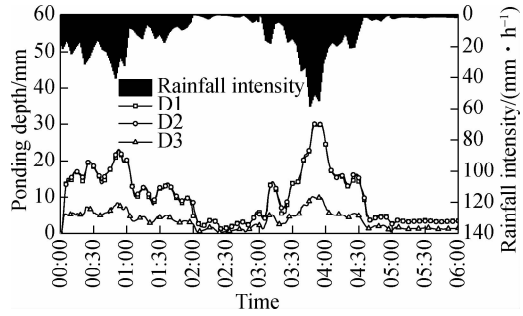

Fig. 4 Variation of ponding depth at curb

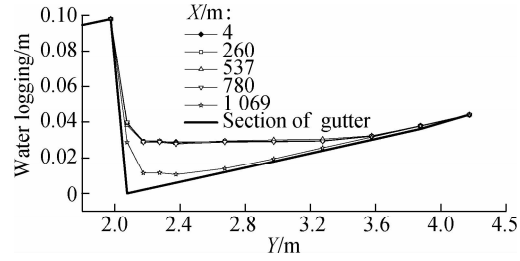

Fig. 5 Ponding width at different transverse sections at 03:49

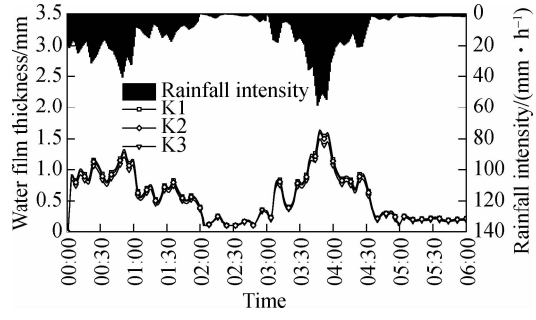

Fig. 6 Variation of lane WFT

Tab. 4 Runoff depth of observation points during the heaviest rainfall time segment

Time	Ponding depth at curb/mm			Lane WFT/mm			Rainfall intensity/ (mm · h⁻¹)
	D1	D2	D3	K1	K2	K3	
03:45	24.18	24.34	9.40	1.49	1.44	1.36	51.90
03:46	26.23	26.43	10.00	1.59	1.55	1.46	58.20
03:47	28.19	28.70	10.20	1.64	1.62	1.50	56.10
03:48	29.43	29.59	10.10	1.62	1.58	1.48	54.00
03:49	29.84	29.99	9.96	1.59	1.55	1.45	51.80
03:50	29.81	29.95	9.82	1.55	1.51	1.42	49.70

for the lane WFT. Hydraulic engineering circular (HEC) 22[16] is widely used in the design of highways and bridges in the US[17]. The sheet flow travel time calculated by HEC-22 method is 1.72 min. The kinematic wave equation with non-optimal coefficients and the simplified momentum equation are used in the HEC-22 method[18], which causes the over-estimation of the sheet flow travel time. According to *General Specifications for Design of Highway Bridges and Culverts* (JTG D60—2015)[19] in China, the sheet flow travel time is 1.75 min, which also over-estimates the sheet flow travel time. It is unfavor-

able to the drainage design of bridge if this time is over-estimated.

We also found that the velocity of the observation points have similar changing laws to the ponding depth at the curb and lane WFT. Thus, this study only presents partial velocity results in Tab. 5 and Tab. 6, which shows that the velocity and runoff depth reach the maximum value at the same time. The curb obstructs the runoff flow of D1 and D2 in the Y direction. Thus, V_y is close to 0. D3 is the observation point directly above an inlet, the runoff can flow into the inlet, so V_y of D3 is not 0. On the other hand, the direction of velocity can be calculated by V_y/V_x. Except for D3, the direction of velocity is almost constant with the rainfall intensity changing. Moreover, the velocity direction of D1 is almost the same as that of D2, which also exists in K1, K2 and K3. Meanwhile, since the longitudinal slope is larger than the traverse slope, the V_y of K1, K2 and K3 is larger than that of V_x.

Tab. 5 Velocity of D1, D2 and D3 m/s

Time	D1		D2		D3	
	V_x	V_y	V_x	V_y	V_x	V_y
03:45	−0.75	0	−0.75	0	−0.35	−0.01
03:46	−0.78	0	−0.79	0	−0.37	−0.01
03:47	−0.80	0	−0.81	0	−0.38	−0.01
03:48	−0.82	0	−0.83	0	−0.38	−0.01
03:49	−0.83	0	−0.83	0	−0.37	−0.01
03:50	−0.83	0	−0.83	0	−0.37	−0.01

Tab. 6 Velocity of K1, K2 and K3 m/s

Time	K1		K2		K3	
	V_x	V_y	V_x	V_y	V_x	V_y
03:45	−0.03	−0.05	−0.03	−0.05	−0.03	−0.05
03:46	−0.04	−0.06	−0.04	−0.05	−0.03	−0.05
03:47	−0.04	−0.06	−0.04	−0.06	−0.03	−0.05
03:48	−0.04	−0.06	−0.04	−0.06	−0.03	−0.05
03:49	−0.04	−0.07	−0.04	−0.05	−0.03	−0.05
03:50	−0.03	−0.05	−0.03	−0.05	−0.03	−0.05

It is summarized that the ponding depth at the curb, lane WFT and velocity rate are positively related to the rainfall intensity. In order to compare their changes in the time dimension, the variation coefficient of the above three runoff parameters is calculated by

$$C_v = \sqrt{\frac{\sum_{i=1}^{n}\left(\frac{U_i}{\bar{U}} - 1\right)^2}{n-1}} \quad (2)$$

where C_v is the dimensionless parameter; U_i is a sample series of one of the runoff parameters; $\bar{U}$ is the mean value of the sample series; n is the length of the data set.

The value of C_v reflects the response degree of runoff parameters to rainfall intensity. In this study, the change of the above three runoff parameters is caused by the change in rainfall intensity. A smaller C_v indicates relatively stable runoff characteristics, and runoff characteristics have a slower response to the rainfall intensity. Conversely, a higher C_v indicates that the runoff characteristics are severely volatile and have a faster response to the rainfall intensity.

Tab. 7 Coefficient of variation of runoff parameters

Observation points	Coefficient of variation C_v					
	D1	D2	D3	K1	K2	K3
WFT				0.68	0.67	0.68
Ponding depth at curb	0.71	0.71	0.69			
Velocity rate	0.66	0.66	0.76	0.79	0.79	0.81
Direction of velocity	0.05	0.05	0.05	0.18	0.18	0.18

It is obvious that the C_v of velocity direction is very low, which indicates that the direction of velocity of runoff is relatively stable. The other three are relatively high, they are volatile and have higher research significance. The C_v of WFT (K1, K2 and K3) is lower than that of ponding (D1, D2 and D3). Meanwhile, for the velocity rate, the C_v of K1, K2 and K3 is higher than that of D1, D2, and D3. This indicates that the WFT of K1, K2 and K3 has relatively weak variability in the time dimension. However, their velocity rates are more volatile than those of D1, D2 and D3.

The simulation results point out that the temporal distribution of bridge deck runoff is changing in real-time, and the runoff parameters have a positive relationship with rainfall intensity; however, their response degrees to rainfall intensity are different, and there are also spatial differences. Furthermore, the typical methods in specifications lead to an over-estimation on the sheet flow travel time.

2.2 The spatial distribution

In order to explore the spatial distribution laws, the result of section L0 and L1 at 03:50 is extracted and demonstrated in Fig. 7. The direction of runoff velocity is relatively stable. Thus, the direction of velocity is not the key. This study focuses on the ponding depth at the curb, the lane WFT and the velocity rate.

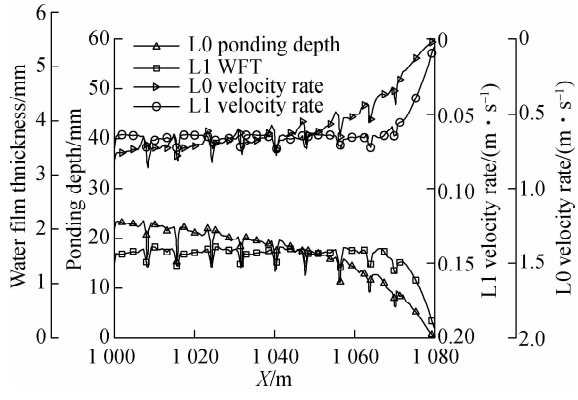

Fig. 7 Results of L0 and L1 along with X at 03:50

Figs. 7 and 8 demonstrate that inlets can affect the runoff distributions, and the changes of the runoff distributions keep stable after rainwater concentrates. W1 (544.23, 5.075) is the observation point above the inlet where the minimum lane WFT occurs, and P2 (546, 2.075) and W2 (546, 5.075) are the observation points where the maximum runoff depth occurs. In order to quantify the inlet's effects on the distribution of bridge deck runoff, the above observation points are extracted to calculate the effect degree.

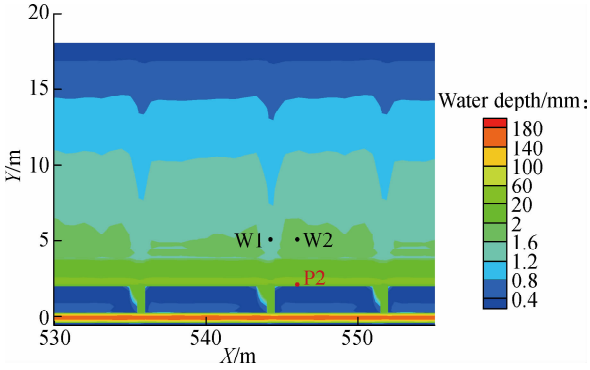

Fig. 8 Spatial distributions of runoff at 03:50

The velocity of sheet flow is calculated by the Chézy equation and Manning equation:

$$V = C\sqrt{RJ} \tag{3}$$

$$C = \frac{1}{n}R^{1/6} \tag{4}$$

where V is the velocity of sheet flow, m/s; C is the Chézy coefficient; R is the hydraulic radius, m; and J is the hydraulic gradient.

The lane WFT and velocity rate can be comprehensively represented by the unit discharge of sheet flow Q_u (m^3/s):

$$Q_u = \frac{1}{n}R^{1.67}J^{0.5} \tag{5}$$

For the sheet flow, R is the lane WFT, and J is the slope of bridge deck.

When two observation points have the same Y coordinates, their unit discharges are equal if there are no inlets on the curb. However, due to the effect of the inlets, their unit discharges are different, and the effect degree of inlet on lane water film m_f(%) is

$$m_f = \frac{Q_{u|X2,Y|} - Q_{u|X1,Y|}}{Q_{u|X2,Y|}} = \frac{h^{1.67}_{|X2,Y|} - h^{1.67}_{|X1,Y|}}{h^{1.67}_{|X2,Y|}} \times 100 \tag{6}$$

where $\{X1, Y\}$ and $\{X2, Y\}$ are the coordinate of observation points; $h_{|X1,Y|}$ and $h_{|X2,Y|}$ are the lane WFT of points, m. In this paper, the two points are W1 and W2, respectively.

The ponding depth at the curb and the velocity rate can be comprehensively represented by the gutter discharge. In accordance with HEC-22 and Schalla's study[20], the interception efficiency of the inlets is a perfect parameter to evaluate the inlet's influence on the ponding at the curb:

$$Q_a = \frac{3}{8}\frac{S_L^{0.5}y_p^{2.67}}{nS_x} \tag{7}$$

$$L_T = 0.817Q_a^{0.42}S_L^{0.3}\left(\frac{1}{nS_x}\right)^{0.6} \tag{8}$$

$$m_d = \left(1 - \left(1 - \frac{L}{L_T}\right)^{1.8}\right) \times 100 \tag{9}$$

where m_d is the effect degree of inlet on the ponding at curb, %; n is the Manning coefficient; S_L is the longitudinal slope; S_x is the transverse slope; y_p is the ponding depth at the curb, m, in this paper, y_p is the ponding depth of P2. Q_a is the gutter flow, m^3/s; L_T is the curb opening length required to intercept 100% of the gutter flow, m; L is the curb opening length, m, and in this paper, L = 0.35 m.

Using Eq. (6) and Eq. (9), m_f and m_d can be calculated. From the comparison in Fig. 9, m_f has a positive relationship with rainfall intensity; when m_d is opposite, the relationship is negative.

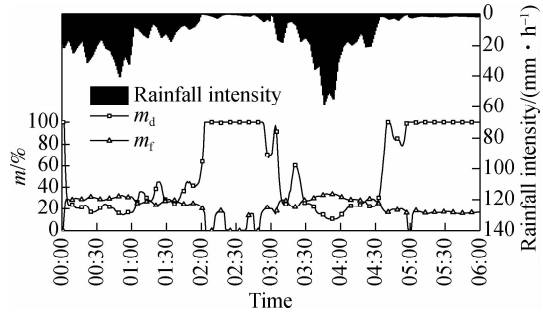

Fig. 9 Variations of m_d and m_f along with time

Based on a large amount of objective data, the regression method is the most representative and it is widely applied when exploring the related law among different parameters. Consequently, it is also used to reflect the trends of m_d and m_f with the changes of rainfall intensity. Fig. 10 illustrates that R^2 (goodness-of-fit) is 0.824 for m_d, and R^2 is 0.706 for m_f for Taizhou Bridge. During a natural rainstorm process, the inlet's effects on lane WFT and the ponding depth at the curb have a nonlinear quantitative relationship with the rainfall intensity.

2.3 Characteristics of bridge approach slab runoff

At the end of bridge, the bridge approach slab is designed for the transition of S_L to prevent bumping. Bridge approach slab runoff is heavy for large span bridges after the rain concentrates. Accordingly, bridge approach slab will come under obvious attack. Ponding with a larger area is one of the significant impacts when S_L decreases.

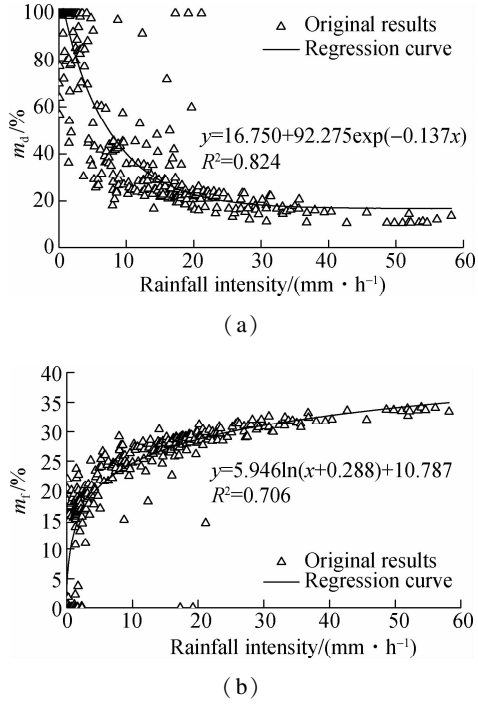

Fig. 10 Performance of regression equations. (a) m_d vs. rainfall intensity; (b) m_f vs. rainfall intensity

In this simulation, the bridge approach slab is divided into three transition segments (from 0 to −15 m in the X direction) and S_L ranges from 2.5% to 0%. T1, T2 and T3 sections in Fig. 11 are used to analyze the runoff distribution with the change of S_L.

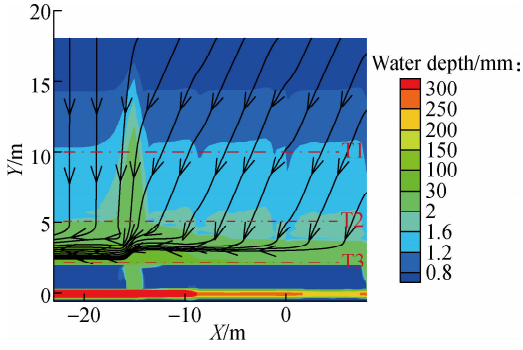

Fig. 11 Flow field of bridge approach slab runoff at 03:49

As depicted in Fig. 11, the streamline field presents a slight change, but it is dramatic at −15 m of X, which indicates that streamline field of bridge approach slab runoff is not sensitive to the change of S_L, but it rapidly changes at the section with the minimum S_L.

As shown in Fig. 12, the ponding depth at the curb (T3) continues to increase from 0 to −15 m in the X direction, especially at the first three slope transition sections, and the rising trend is sharp. Then, the ponding depth at the curb decreases close to −15 m of X due to a large inlet. The results indicate that the ponding depth at curb is significantly sensitive to the change of S_L and increases from 30.12 to 58.14 mm. Thus, an effective drainage design is necessary at the bridge approach slab. On the other hand, the lane WFT (T1 and T2) only has a precipitous change near −15 m of X, and the maximum lane WFT is 3.26 mm, which indicates that lane WFT is sensitive to the location with the minimum S_L. Except for the zone of sudden change, the lane WFT changes little; the lane WFT of T1 is about 1.25 mm; and that of T2 is about 1.61 mm. Thus, the lane WFT is insensitive to the gradual change of S_L, which is consistent with the conclusion of Ref. [4].

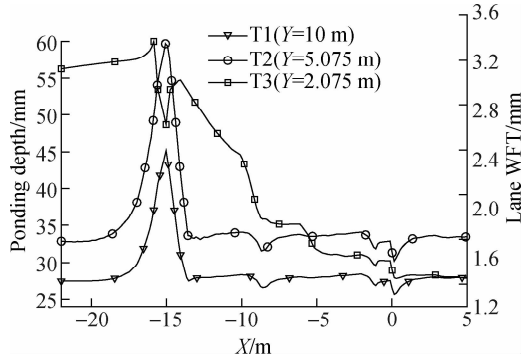

Fig. 12 Runoff depth at 03:49 with variation of T1, T2 and T3

3 Conclusions

1) The runoff depth and velocity rate show a positive relationship with the rainfall intensity; however, there are some differences in their response degrees to it. The obvious spatiotemporal differences are shown in the characteristics of bridge deck runoff.

2) With the change in the rainfall intensity, the inlet's effect degree on lane water film can be described as a natural logarithm function ($R^2 = 0.706$). Yet, the inlet's effect degree on the ponding at the curb can be illustrated as a negative exponential function ($R^2 = 0.824$). The inlet's effects on bridge deck runoff show a good quantitative relationship with the rainfall intensity.

3) At the bridge approach slab, the lane WFT is insensitive to the change of S_L, but it significantly increases at the location with the minimum S_L. Conversely, the ponding depth at the curb is very sensitive to the change of S_L. The effective drainage measures are necessary, and the location with the minimum S_L needs to be paid sufficient attention at the bridge approach slab.

References

[1] Luo J, Liu J B, Wang Y Q, et al. Validation test on pavement water film depth prediction model[J]. *China Journal of Highway & Transport*, 2015, **28**(12): 57 − 63. http://zgglxb.chd.edu.cn/CN/Y2015/V28/I12/57. (in Chinese)

[2] Ma Y, Geng Y, Chen X, et al. Prediction for asphalt pavement water film thickness based on artificial neural network[J]. *Journal of Southeast University (English Edition)*, 2017, **33**(4): 490 − 495. DOI: 10.3969/j.

issn. 1003-7985. 2017. 04. 016.
[3] Chen F P. Study on the theoretical calculation model of rain water depth on road surface[J]. *Modern Transportation Technology*, 2014, **11**(3): 12 - 15. http://www.cqvip.com/read/read.aspx? id=50269212. (in Chinese)
[4] Zhang L, Zhang Z. Impact of road slope on water film thickness[J]. *Journal of Chongqing Jiaotong University (Natural Sciences)*, 2013, **32**(3): 404 - 406. DOI: 10.3969/j.issn.1674-0696.2013.03.08. (in Chinese)
[5] Staufer P, Siekmann M, Loos S, et al. Numerical modeling of water levels on pavements under extreme rainfall [J]. *Journal of Transportation Engineering*, 2012, **138**(6): 732 - 740. DOI: 10.1061/(ASCE)TE.1943-5436.0000373.
[6] Herrmann S R. Simulationsmodell zum wasserabfluss-und aquaplaning-verhalten auf fahrbahnoberflächen [D]. Universität Stuttgart: Veröffentlichungen aus dem Institut für Straßen-und Verkehrswesen, 2008: 48 - 68. DOI: 10.18419/opus-277.
[7] Cristina C M, Sansalone J J. Kinematic wave model of urban pavement rainfall-runoff subject to traffic loadings [J]. *Journal of Environmental Engineering*, 2003, **129**(7): 629 - 636. DOI: 10.1061/(ASCE)0733-9372(2003)129:7(629).
[8] Chen L, Battaglia F, Flintsch G W, et al. Highway drainage at superelevation transitions by 3-D computational fluid dynamics modeling[R/OL]. *Transportation Research Board*, 2017. https://trid.trb.org/view.aspx? id=1437588.
[9] Tan S A, Fwa T F, Chai K C. Drainage considerations for porous asphalt surface course design[J]. *Transportation Research Record: Journal of the Transportation Research Board*, 2004, **1868**: 142 - 149. DOI: 10.3141/1868-15.
[10] Gómez M, Recasens J, Russo B, et al. Assessment of inlet efficiency through a 3D simulation: Numerical and experimental comparison[J]. *Water Science and Technology*, 2016, **74**(8): 1926 - 1935. DOI: 10.2166/wst.2016.326.
[11] Charbeneau R J, Jeong J, Barrett M E. Highway drainage at superelevation transitions[R/OL]. *Highway Design*, 2008. http://www.utexas.edu/research/ctr/pdf_reports/0_4875_1.pdf.
[12] Jeong J, Charbeneau R J. Diffusion wave model for simulating storm-water runoff on highway pavement surfaces at superelevation transition[J]. *Journal of Hydraulic Engineering*, 2010, **136**(10): 770 - 778. DOI: 10.1061/(ASCE)HY.1943-7900.0000253.
[13] Ressel W, Wolff A, Alber S, et al. Modelling and simulation of pavement drainage[J]. *International Journal of Pavement Engineering*, 2017(2): 1 - 10. DOI: 10.1080/10298436.2017.1347437.
[14] Chen X H, Geng Y F, Jiang Q L, et al. Innovative approach for pavement runoff characterization[J]. *Journal of Performance of Constructed Facilities*, 2017, **31**(5): 04017047. DOI: 10.1061/(ASCE)CF.1943-5509.0001045.
[15] Guo X, Wu Z, He H, et al. Variations in the start, end, and length of extreme precipitation period across China [J]. *International Journal of Climatology*, 2017(12). DOI: 10.1002/joc.5345.
[16] Brown S A, Schall J D, Morris J L, et al. Urban drainage design manual. Hydraulic engineering circular 22, No. NHI-01-021 HEC-22[R/OL]. Washington, DC, USA: Federal Highway Administration (FHWA), 2009. https://www.fhwa.dot.gov/engineering/hydraulics/library_arc.cfm? pub_number=22&id=140.
[17] Qian Q, Liu X Y, Barrett M E, et al. Physical modeling on hydraulic performance of rectangular bridge deck Drains[J]. *Water*, 2016, **8**(2): 67. DOI: 10.3390/w8020067.
[18] McCuen R H, Spiess J M. Assessment of kinematic wave time of concentration[J]. *Journal of Hydraulic Engineering*, 1995, **121**(3): 256 - 266. DOI: 10.1061/(ASCE)0733-9429(1995)121:3(256).
[19] Ministry of Transport of the People's Republic of China. JTG D60—2015 General specifications for design of highway bridges and culverts[S]. Beijing: China Communications Press, 2015. (in Chinese)
[20] Schalla F E, Ashraf M, Barrett M E, et al. Limitations of traditional capacity equations for long curb inlets[J]. *Transportation Research Record: Journal of the Transportation Research Board*, 2017, **2638**: 97 - 103. DOI: 10.3141/2638-11.

桥面径流的时空分布特性

耿艳芬　柯　兴　郑　鑫

(东南大学交通学院,南京 210096)

摘要:探究了桥面径流在自然降雨过程中的时空特性.以泰州大桥为例,采用基于二维浅水方程的水动力学数值模型对桥面径流进行模拟分析.结果表明,桥面径流流速和水深与雨强成正相关关系,但两者对雨强的响应度不同.泄水口对路面水膜的影响度与雨强成正相关,该关系可由自然对数函数表示($R^2=0.706$);泄水口对路肩积水的影响度与雨强成负相关,该关系可由负指数函数表示($R^2=0.824$).在桥台搭板处,随纵坡 S_L 减小,路肩积水深度显著增加,路面水膜厚度基本保持不变,但路面水膜厚度在最小纵坡处发生明显增加.由此得出结论,桥面径流分布有明显的时空差异性,泄水口对桥面径流的影响度与雨强之间存在较强的非线性关系,桥台搭板处需设置高效的排水设施.

关键词:二维浅水方程;桥面径流;时空特性;路肩积水;路面水膜

中图分类号:U416.2